Mechanical Softness of Ferroelectric 180° Domain Walls

Christina Stefani,[1] Louis Ponet,[2,3] Konstantin Shapovalov,[4] Peng Chen,[2] Eric Langenberg,[5] Darrell G. Schlom,[5,6] Sergey Artyukhin,[2] Massimiliano Stengel,[4,7] Neus Domingo,[1] and Gustau Catalan[1,7]

[1]*ICN2-Institut Català de Nanociència I Nanotecnologia (CERCA-BIST-CSIC), Campus Universitat Autònoma de Barcelona, Bellaterra, Catalonia, Spain*
[2]*Italian Institute of Technology, 16163 Genoa GE, Italy*
[3]*Scuola Normale Superiore di Pisa, 56126 Pisa PI, Italy*
[4]*ICMAB-Institut de Ciència de Materials de Barcelona, Bellaterra, Catalonia, Spain*
[5]*Department of Materials Science and Engineering, Cornell University, Ithaca, New York 14853, USA*
[6]*Kavli Institute at Cornell for Nanoscale Science, Ithaca, New York 14853, USA*
[7]*ICREA-Catalan Institution for Research and Advanced Studies, Passeig Lluïs Companys, Barcelona, Catalonia, Spain*

(Received 23 January 2020; revised 19 June 2020; accepted 17 July 2020; published 1 October 2020)

Using scanning probe microscopy, we measure the out-of-plane mechanical response of ferroelectric 180° domain walls and observe that, despite separating domains that are mechanically identical, the walls appear mechanically distinct—softer—compared to the domains. This effect is observed in different ferroelectric materials ($LiNbO_3$, $BaTiO_3$, and $PbTiO_3$) and with different morphologies (from single crystals to thin films), suggesting that the effect is universal. We propose a theoretical framework that explains the domain wall softening and justifies that the effect should be common to all ferroelectrics. The lesson is, therefore, that domain walls are not only functionally different from the domains they separate, but also mechanically distinct.

DOI: 10.1103/PhysRevX.10.041001 Subject Areas: Materials Science

I. INTRODUCTION

An important part of the appeal of domain walls resides in the functional contrast between their properties and those of the domains they separate. Multiferroic $BiFeO_3$ displays conductivity and magnetoresistance at its domain walls [1–4], despite being an insulator wide-band-gap semiconductor, and the [5] ferroelastic domain walls of semiconductor WO_{3-x} are superconducting [6]. Electrical conductance is also measured in the ferroelectric domain walls $Pb(Zr_{0.2}Ti_{0.8})O_3$ [7], $LiNbO_3$ [8], and $BaTiO_3$, as well as those of multiferroic $YMnO_3$ [9] and $Cu_3B_7O_{13}Cl$ [10]. Their distinct functionality, nanoscopic thickness, and the fact that they can be created, shaped, or moved by an external field is fueling the field of "domain wall nanoelectronics," where domain walls are regarded as mobile two-dimensional electronic elements [11–13].

In contrast to the vigorous research on domain wall functionality, less is known about their mechanical properties. This difference is partly explained by the difficulty of isolating the mechanical response of individual walls, which are atomically thin structures sandwiched between much wider domains that dominate the overall mechanical behavior. All the same, the mechanical response of domain walls matters. For one thing, mechanical stress is one of the mechanisms by which domain walls can be moved: Ferroelectric-ferroelastic domain walls respond to stress [14], affecting the overall dielectric, piezoelectric, and elastic properties of ferroelectric ceramics as well as their lability [15] and fracture physics [16,17]. Even purely ferroelectric (i.e., nonferroelastic) domain walls also react to strain gradients introduced by external indentation [18] or by the proximity of another ferroelectric (nonferroelastic) domain wall [19]. Moreover, elastic contrast between domains and domain walls may affect the propagation and scattering of phonons—and, consequently, also the propagation of heat [20–22]. Also, if there is mechanical contrast in 180° domain walls, it may be used as an alternative way to mechanically read ferroelectric bits [23].

The interplay between domain wall motion or domain reconfiguration and the overall mechanical and electromechanical properties of ferroelectric devices is well documented [24–29]. In contrast, there is barely any knowledge of the internal deformation mechanics of the individual walls themselves—particularly for nonferroelastic 180° walls separating antiparallel ferroelectric domains. A seminal investigation by Tsuji *et al.* shows that the 180° domain walls of ferroelectric Lead zirconate titanate

ceramics appear softer than the domains when probed by atomic force microscopy [30,31]. However, it is not obvious why such domain walls should display any mechanical contrast, given that the polar axis is the same on both sides of the wall and, thus, the domains on either side are mechanically identical (unlike in ferroelastic 90° domains, where the spontaneous strain axis is different on both sides of the wall, so the mechanical properties must necessarily change across the wall). The present investigation therefore seeks to (i) determine whether domain wall mechanical contrast is a general property of 180° ferroelectric domains, (ii) quantify its magnitude, and (iii) propose a theoretical explanation for its physical origin. We find that the effect is general, quantitatively significant, and physically inevitable.

Besides its fundamental interest, this discovery has practical ramifications not only for the mechanics of ferroelectrics but also for their functionality. The mechanical detection of ferroelectric domain walls means that they can be probed in a voltage-free manner, which may be convenient for conducting ferroelectrics. Also, as mentioned, heat transport is intimately linked to mechanics, because heat is carried by phonons, which are strain waves. If the lattice is softer at the wall, the phonon speed will be slower, and, hence, effects like phonon refraction or even total internal reflection may be expected; in this context, 180° domain walls could conceivably act as "phonon waveguides" where heat travels along the wall with little dissipation. Since ferroelectric 180° walls can be created or destroyed by voltage (by writing or erasing domains), this result suggests the possibility of using voltage to fabricate periodic and reconfigurable metamaterials with a regular pattern of internal elastic contrast. Put another way, periodically poled ferroelectric crystals, which are already in use for photonic applications [32], may also turn out to be phononic crystals.

II. SAMPLES AND DOMAIN STRUCTURE

We characterize the mechanical properties of domain walls in ferroelectric single crystals of $LiNbO_3$ and $BaTiO_3$ and thin films of $PbTiO_3$. The spread of materials and sample morphologies is chosen in order to determine the generality of the findings. The measurements are based on contact resonance frequency microscopy mode (CRFM). CRFM is a scanning probe microscopy technique that maps, with nanoscopic resolution, the resonance frequency of an AFM tip in contact with the material; higher resonance frequencies correlate with stiffer contact areas, and, conversely, lower resonance frequencies indicate that the material is softer [33]. Additional details about the experimental techniques can be found in Supplemental Material [34]. As we show, besides imaging, this technique can be used to extract quantitative information about differences in the Young's modulus of the material.

Figure 1 shows the piezoresponse force microscopy (PFM) [35,36] images of the ferroelectric domains, showing the 180° phase contrast of oppositely polarized domains. Figure 1 also demonstrates the mechanical response of domain walls as detected by CRFM. In this technique, the tip is in contact with the sample, but it does not excite the sample electrically, as in PFM, but mechanically, through a piezo element placed at the base of the cantilever. In another common experimental setup for CRFM measurements, the sample is vibrated instead of the cantilever, using an acoustic stage underneath it. We perform experiments with both types of experimental setup to verify that the results are equivalent (see Supplemental Material [34]).

The mechanical excitation of the tip induces a local vibration at the contact with the sample, and the frequency of the oscillation is modulated until mechanical resonance is reached. The resonance frequency of the system depends on both the geometrical characteristics of the tip and the tip-sample mechanical contact characteristics. Since the tip is the same throughout the whole measurement, and the force between the tip and sample is also kept constant, changes of resonant frequency, therefore, indicate the changes in the stiffness of the sample, and a lower resonance frequency means a softer material. In all the measurements, noncoated doped Si tips are used. For CRFM images, the tip is grounded during the measurements in a short-circuit configuration, allowing for polarization charge screening.

The first sample tested is a congruent $LiNbO_3$ single crystal, periodically poled with polarization perpendicular to the surface. This material is a uniaxial ferroelectric, so the only domains allowed by symmetry are 180° domains of antiparallel polarization. The antiparallel domain configuration is verified by the phase contrast in the PFM image [Fig. 1(a)]. The size of each domain is approximately 4 μm. From CRFM response of the same area, we observe that the domain walls are markedly darker (i.e., display lower resonance frequency and are, therefore, softer) than the domains.

We also look at a $BaTiO_3$ single crystal, which is considered an archetype of perovskite ferroelectrics. The tetragonal structure of $BaTiO_3$ allows for both antiparallel (180°) and perpendicular (90°) domain configurations, the latter being ferroelastic in addition to ferroelectric. In Fig. 1(b), the PFM image shows the areas with opposite out-of-plane polarization forming 180° ferroelectric domain walls. In the same area, CRFM measurement demonstrates again a downward frequency shift between the domain and domain walls, indicating that in this material domain walls are also mechanically softer than domains.

Finally, we also investigate a $PbTiO_3$ thin film of 50 nm thickness epitaxially grown by reactive molecular beam epitaxy on a single-crystal $SrTiO_3$ substrate (the growth details can be found elsewhere [20]). Because of the large compressive stress exerted by the substrate (−1.36%), only domains with vertical (out-of-plane) polarization

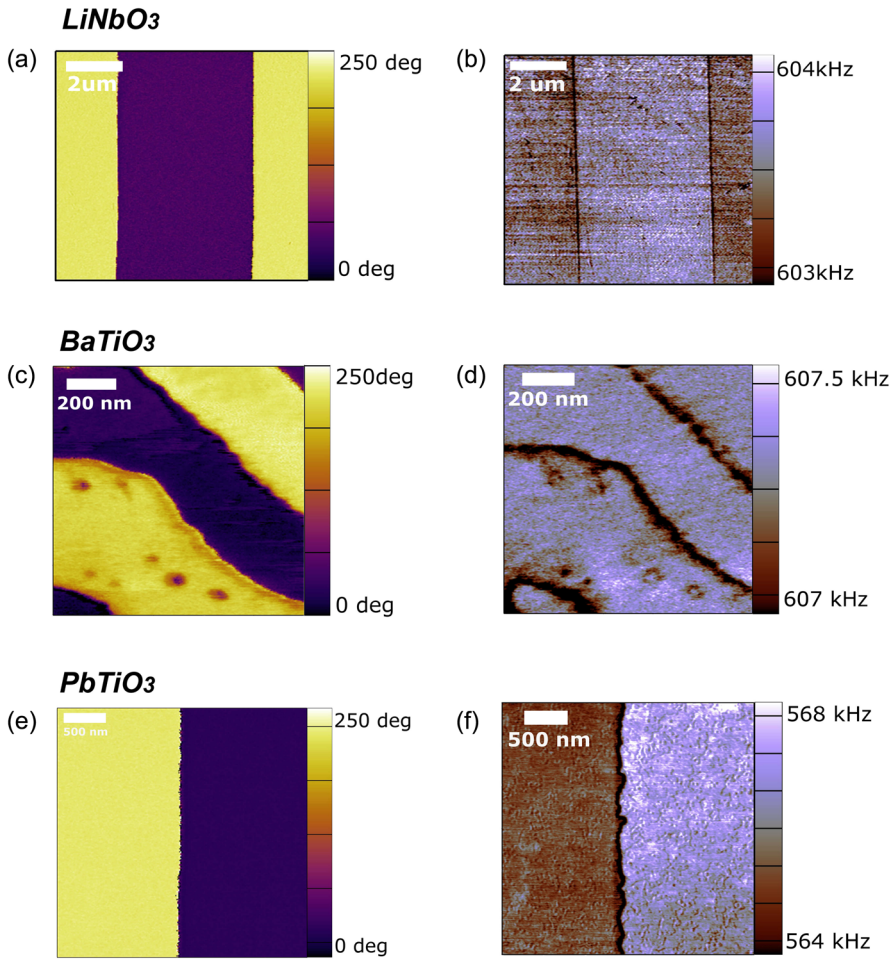

FIG. 1. (a),(b) Periodically poled $LiNbO_3$ single crystal, (c),(d) $BaTiO_3$ single crystal spontaneously polarized, and (e),(f) $PbTiO_3$ thin film. PFM images (a),(c),(e) show the opposite polarization of out-of-plane domains, and CRFM images (b),(d),(f) demonstrate changes in the frequency between domains and domain walls.

are allowed in the ferroelectric film [20]. After electrically polarizing two different areas of the film with a dc voltage of 5 V, we pole domains of opposite sign, as indicated by the corresponding PFM phase contrast [Fig. 1(c)]. Again, the 180° domain walls are observed to be softer than the surrounding domains [Fig. 1(e)]. The relative softness of ferroelectric domain walls, therefore, appears to be a general phenomenon that does not rely on composition or sample morphology.

The observed softening of 180° domain walls is qualitatively similar for all the samples, irrespective of whether the domains are artificially written, such as in $PbTiO_3$ or $LiNbO_3$, or spontaneous, as in the $BaTiO_3$ crystal. Quantitative differences in the resonance frequency shift of the different materials reflect differences in their mechanical properties. However, quantitative conversion from resonance frequency to contact stiffness requires calibration for each individual material, as we demonstrate in this paper. Quantitative analysis is possible only within different regions of the same sample measured with the same cantilever, while comparison between different materials can only be qualitative (further discussion in Supplemental Material [34]).

It has been proposed that some ferroelectric domain walls can be non-Ising type and, thus, have an in-plane component of the polarization [37–40]. We have no experimental evidence for this proposal being the case in the $BaTiO_3$ walls, but the possibility of a mechanical contribution coming from in-plane polarization at the walls is excluded, because in-plane polarization leads to a stiffer, not softer, response (see the higher resonance frequency of the ferroelastic *a* domains in Fig. 3).

The possibility of softening due to local switching effects is also ruled out. Although it is expected that the coercive field of the ferroelectric should be smaller near the ferroelectric wall [41], repeated scans over the same area show no evidence of switching of the polarization: We see no detectable shift in the position of the domain walls even after ten scans with the maximum mechanical load of 20 micro-Newtons (see Supplemental Material [34] and Fig. 4). Although there is no permanent switching, there can be, however, an elastic deflection of the wall toward the

tip, and this deflection is the basis for the theoretical model depicted in Fig. 4.

It is worth mentioning that there is also a small mechanical contrast (small difference in CRFM) between the up and down domains. This contrast is attributed to the coupling of tip-induced flexoelectricity and domain ferroelectricity, which induces an asymmetry in the mechanical response of domains of opposite polarity and is proposed as a mechanism for voltage-free mechanical reading of polarity [23,42,43]. The domain walls, however, are softer than both up- and down-polarized domains, so their softening cannot be explained by this polarity-dependent mechanism.

III. EXPERIMENTAL QUANTIFICATION OF DOMAIN WALL ELASTICITY

In order to quantify the softening, we need to translate the shifts in resonance frequency into changes of stiffness. The system can be described as a system of two springs in series [Fig. 2(a)]: the cantilever itself, with its flexural elastic constant, and the tip-surface contact, which can be described by the Hertzian contact model [44,45] [Fig. 2(b)]. The force applied by the tip is kept constant by a feedback loop, so the contact can also be effectively described as a flat punch determined only by the constant contact radius α [Fig. 2(c)], measured experimentally. The tip-surface contact also acts as two springs in series, corresponding to the tip and the sample, respectively. The effective Young's modulus of the tip-surface system, E^*, is therefore given by

$$\frac{1}{E^*} = \frac{(1-v_s^2)}{E_s} + \frac{(1-v_{\mathrm{tip}}^2)}{E_{\mathrm{tip}}}, \tag{1}$$

where E_s, E_{tip}, v_s, and v_{tip} are the Young's modulus and the Poisson ratios of the sample and the tip, respectively. E^* is related to the contact stiffness k^* as

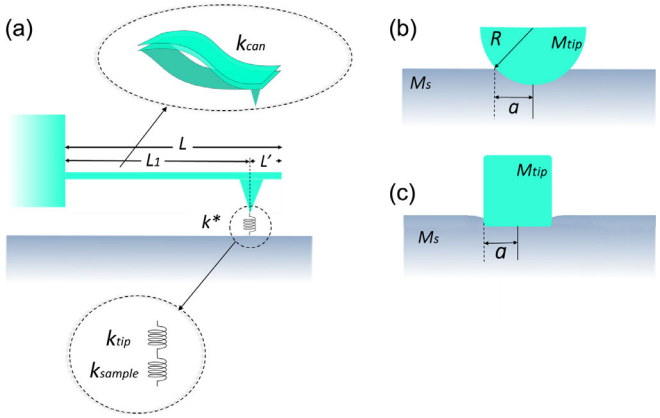

FIG. 2. (a) Schematic presentation of AFM cantilever and tip-sample contact being simulated by a spring with constant k^*. (b) Diagram of tip-sample contact based on a Hertzian mechanical contact model and (c) flat punch contact between the tip and the sample.

$$E^* = \frac{k^*}{2a}. \tag{2}$$

k^* is the elastic constant of the spring that represents the tip-sample interaction [46], also known as contact stiffness, and, like E^*, k^* depends on the stiffness of the tip (k_{tip}) and the stiffness of the sample (k_s).

The quantity we are after is the Young's modulus of the sample (E_s), which we could, in principle, calculate by substracting E_{tip} from E^* in Eq. (1). The problem is that we know neither E^* nor E_{tip}, so we have one equation [Eq. (1)] with three unknowns. To solve this problem, we (i) measure the resonance frequencies of the cantilever and relate them to E^* via elastic theory and (ii) measure the mechanical response of a part of the sample for which E_s is known (in our case, the c-oriented $BaTiO_3$ domains) and use it for calibration. Knowing E^* and E_s allows us to extract E_{tip} and then repeat the analysis on the part of sample for which E_s is unknown—the domain walls. An additional experimental factor that has to be taken into account is the stiffness of the cantilever. In order to mechanically characterize stiff materials, we need cantilevers that are also as stiff as possible, because otherwise all the mechanical deformation takes place in the cantilever rather than in the sample. This factor is illustrated in Supplemental Material [34], where we compare the CRFM results using cantilevers of different stiffness.

Based on the models of Hurley [47] and Rabe, Kopycinska-Müller, and Hirsekorn [48], the cantilever is modeled as a beam with length L, width w, thickness b, density ρ, and Young's modulus E_{can}. The tip is located at a distance $L_1 < L$ from the clamped end of the cantilever, and the remaining distance to the other end of the cantilever is L' [Fig. 2(a)] [47]. The spring constant of the cantilever is calibrated experimentally by measuring force-displacement curves and the free resonance frequency (first harmonic $\mathbf{f}_1^0$) of the cantilever. These parameters are shown in Table I.

The experimental values of free resonance frequency (f_1^0) (i.e., the resonance frequency when the tip of the cantilever is suspended above the sample without touching it) and the contact resonance frequency (f_1) (i.e., the resonance frequency when the tip is in contact with the

TABLE I. Geometrical characteristics of the cantilever, experimental values of the free resonance frequency, and contact resonance frequencies for a and c domains of bulk $BaTiO_3$ and the corresponding wavelengths as calculated by Eqs. (1) and (2). The experimental value of the cantilever's spring constant (k_{lever}) and the calculated normalized contact stiffness k^*/k_{lever} of the system.

L (μm)	b (μm)	ρ (g/cm^3)	L_1 (μm)	$\mathbf{f}_1^0$ (kHz)	E_{can} (GPa)	$\mathbf{k}_{\mathrm{lever}}$ (N/m)	α (nm)
220	6,5	2,33	211,2	158	170	38	7

sample) are used to relate the corresponding wave numbers (x_i) through the equation [47]

$$x_1 L = x_1^0 L \sqrt{\frac{f_1}{f_1^0}}, \tag{3}$$

where the free cantilever wave number x_1^0 is given by [47]

$$(x_1^0 L)^2 = 4\pi f_1^0 \frac{L^2}{b}\sqrt{\frac{3\rho}{E_{\text{can}}}}. \tag{4}$$

The normalized contact stiffness $k*/k_{\text{lever}}$ is then given by [33,49]

$$\frac{k^*}{k_{\text{lever}}} = \frac{2}{3}(x_1 L_1)^3 \frac{(1+\cos x_1 L \cosh x_1 L)}{D}, \tag{5}$$

$$\begin{aligned} D = {} & (\sin x_1 L' \cosh x_1 L' - \cos x_1 L' \sinh x_1 L') \\ & \times (1 - \cos x_1 L_1 \cosh x_1 L_1) \\ & - (\sin x_1 L_1 \cosh x_1 L_1 - \cos x_1 L_1 \sinh x_1 L_1) \\ & \times (1 + \cos x_1 L' \cosh x_1 L'). \end{aligned} \tag{6}$$

The equations above connect the contact resonance frequencies and cantilever's spring constant to the contact stiffness k^* and, hence, using Eq. (2), to the contact's effective Young's modulus E^*. If the sample's Young's modulus E_s is also known (as it is for c-oriented barium titanate [50]), we can now use Eq. (1) to calculate the tip's Young's modulus (E_{tip}). The calculation can then be repeated on the domain wall, where E_s is not known but E_{tip} is. The results of the calculations are shown in Table II.

Considering the experimental results and using the model described above, the shift in resonance frequency of domain walls corresponds to a reduction of the effective Young's modulus of approximately 19%, with respect to the Young's modulus of the c domains.

IV. THEORY OF FERROELECTRIC DOMAIN WALL SOFTENING

Having determined that the domain walls are mechanically softer than the domains despite being ferroelectric and not ferroelastic, the next question is why. In their seminal work, Tsuji *et al.* [30] put forward three hypotheses: (i) defects, which are known to be attracted to domain walls, (ii) dynamic softening due to ferroelectric switching near the wall, and (iii) reduced depolarization energy at the domain wall, where there is no piezoelectricity. Let us examine these possibilities.

TABLE II. Young's modulus of $BaTiO_3$ based on the literature [50] (E_s) and experimental results for c domains of $BaTiO_3$ as used to calibrate the Young's modulus of the tip (E_{tip}). For domain walls, all the experimental values and the derived values of the Young's modulus.

	$\mathbf{f}_1$ (kHz)	$\mathbf{k}^*/\mathbf{k}_{\text{lever}}$	v_s	E^* (GPa)	E_s (GPa)
c domains	738,5	239,92	0,3	17,07	63,6
Domain walls	737	239,48	0,25	0,45	51,2

Defects are sample dependent, and common ones, such as oxygen vacancies, are notoriously difficult to quantify. The weakening of interatomic bonds caused by a vacancy should be fairly isotropic or at least orthotropic in the nearly cubic perovskite structure. That is to say, the defect-induced softening of the 180° walls should be similar in the in-plane and out-of-plane directions. We compare the mechanical contrast of 180° walls inside the a domains (polarization in plane) with those in the c domains (polarization out of plane) for the $BaTiO_3$ crystal, where both polarizations are accessible in a single scan due to the existence of a-c twins as well as 180° walls [Fig. 3(a)]. As Fig. 3(b) shows, while for c domains (bubble domains) the 180° walls are softer, when the bubble domains penetrate into the a domains (in-plane polarization), the mechanical contrast of the 180° walls disappears. The disappearance of mechanical contrast when the polarization is in plane, combined with the fact that we observe the softening of out-of-plane walls in materials with different chemistries, leads us to believe that the role of chemical defects is less important than the out-of-plane orientation of the polarization.

The strain fields of a multidomain ferroelectric under the tip pressure is a mesoscopic problem too challenging for first-principles atomistic calculations. Instead, we resort to a continuum model, with parameters for $BaTiO_3$ determined by previous first-principles work [51,52]. The starting point is the free-energy density of the system, which can be described by the Ginzburg-Landau-Devonshire model [51,52]:

$$f = f_l + f_g + f_q + f_c + f_f + f_{\text{electr}}, \tag{7}$$

$$f_l = a_{ij}P_iP_j + a_{ijkl}P_iP_jP_kP_l + a_{ijklmn}P_iP_jP_kP_lP_mP_n, \tag{8}$$

$$f_g = G_{ijkl}\nabla_i P_j \nabla_k P_l/2, \tag{9}$$

$$f_q = -q_{ijkl}P_iP_j\varepsilon_{kl}, \tag{10}$$

$$f_c = C_{ijkl}\varepsilon_{ij}\varepsilon_{kl}/2, \tag{11}$$

$$f_f = \frac{\Gamma_{ijkl}}{2}(\nabla_i P_j \varepsilon_{kl} - P_i \nabla_j \varepsilon_{kl}), \tag{12}$$

$$f_{\text{electr}} = \epsilon_r E^2, \tag{13}$$

where f_l is the Landau free-energy density for uniform ferroelectric polarization P, f_g describes the energy penalty

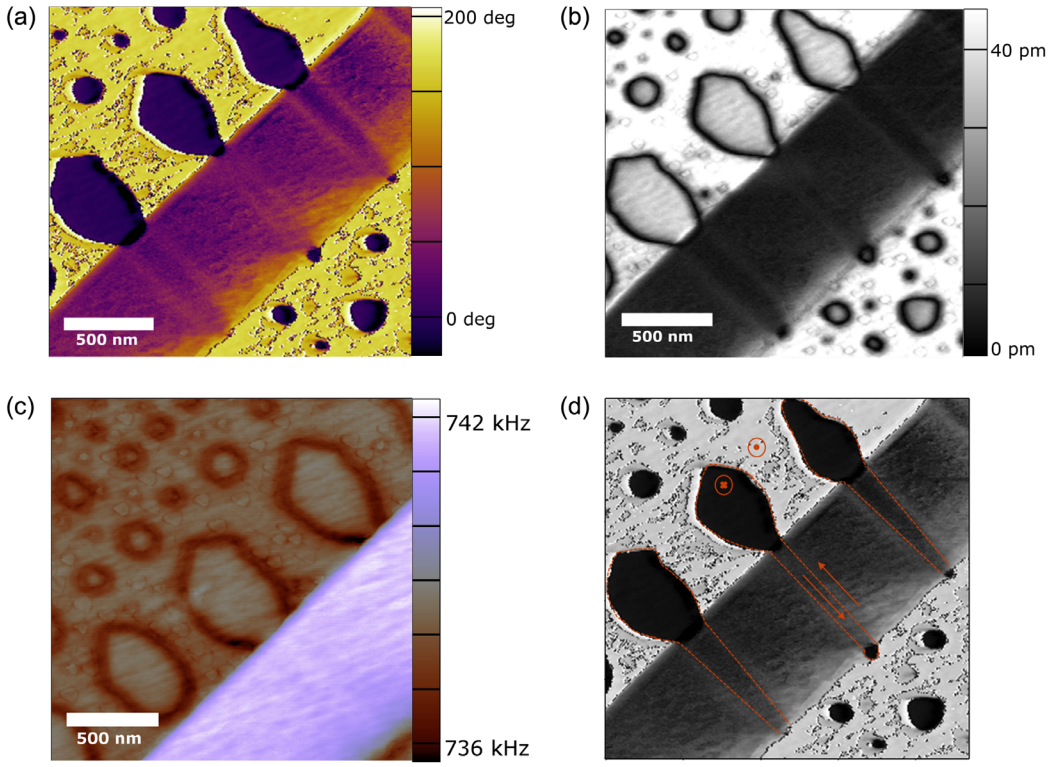

FIG. 3. (a) Vertical PFM phase of $BaTiO_3$ single crystal spontaneously polarized, where the opposite out-of-plane polarization of the crystal is shown. (b) Vertical PFM amplitude of the crystal, where the in-plane polarization is denoted. (c) CRFM image of the same area where there is no difference in frequency contrast due to in-plane polarization. (d) Schematic representation of in-plane polarization.

for spatial variations of P, f_q describes the interaction between the polarization and strains ε_{ij} (electrostriction), and f_c is the elastic free-energy density, while f_f denotes the contribution from flexoelectricity, the interaction between strain gradients and the polarization. Γ_{ijkl} is the flexoelectric tensor. The strain ε_{ij} is defined as $\frac{1}{2}(\nabla_i u_j + \nabla_j u_i)$, where u are the displacements; summation over repeated indices is implied.

The integral of the free-energy density over the entire crystal is minimized in the equilibrium situation. The electrostriction term f_q generates a spontaneous tensile strain along the polar direction inside the ferroelectric domains. This tensile strain is locally reduced at the wall due to the absence of polarization, which leads to a depression in the surface centered at the wall, as demonstrated in Fig. 4(b). The compressive pressure from CRFM tip interacts with this preexisting compressive strain profile. The result is that the wall moves toward the tip, so that the domain wall depression coincides with the locum of the tip compression.

Pinning of the domain wall by the disorder potential and Peierls-Nabarro barriers results in a complex response. In the strong pinning regime, the wall bends only toward the tip. This effect can be qualitatively captured by a simple free-energy expansion, with a flat domain wall (DW) interacting with a parabolic pinning potential (second term), and the tip located at x_{tip} and applying the force F_z:

$$E = E_0 - F_z u_z(x_{\mathrm{tip}} - x_{\mathrm{DW}}) + \frac{m\omega^2 x_{\mathrm{DW}}^2}{2}. \qquad (14)$$

Expanding the surface profile in small x_{DW} and minimizing the energy with regards to x_{DW}, we obtain $x_{\mathrm{DW}} = -Fu'(x_{\mathrm{tip}})/m\omega^2$, to the first order in F. The correction to the compliance is then $\Delta c = u'(x_{\mathrm{tip}})^2/(m\omega^2)^2$. Hence, for significant softening, it is crucial that $u'(x_{\mathrm{tip}})$ is large, leading to an increased effect when pressing within the DW strain footprint.

If the force applied by the tip is large enough to overcome the pinning potential, the wall slides toward the tip, leading to a strongly nonlinear effect. These domain wall sliding modes usually have a frequency in the gigahertz range [53–55]. As the domain wall's "strain-hollow" slides toward the AFM tip, the AFM registers a relatively large deformation in response to the stress and, thus, a low effective stiffness (see Fig. 4). To quantify this effect, it is necessary to solve the free energy in Eqs. (7)–(13), which is analytically intractable but can be numerically computed by finite elements. We perform finite element simulations using known parameters from previous first-principles

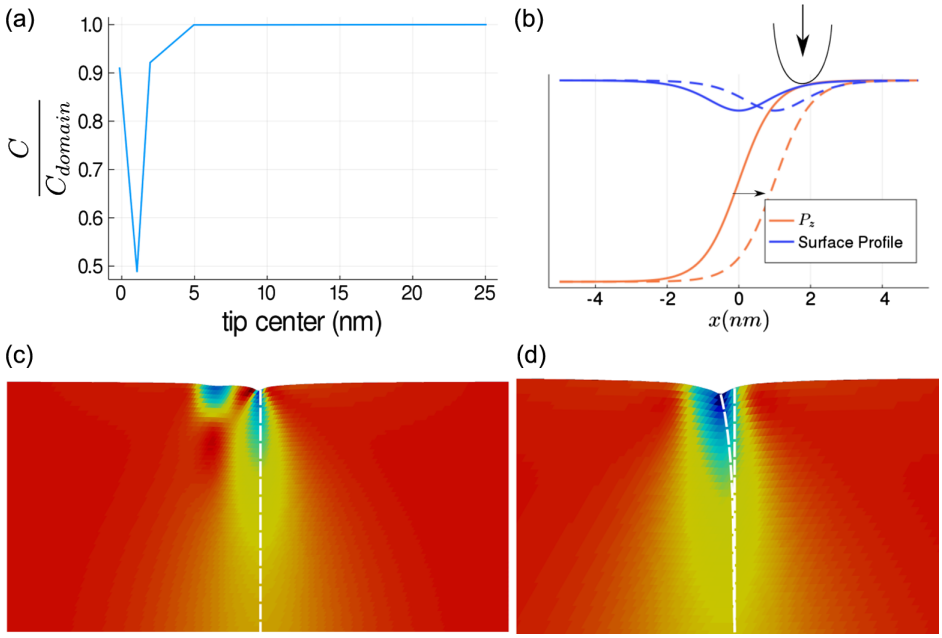

FIG. 4. (a) Simulated change of stiffness as a function of the distance between the CRFM tip and a domain wall. The softening is maximized slightly away from the domain wall, but within its strain footprint, where the DW sliding mode contribution is important. The experimental situation corresponds to averaging within the tip region. (b) Schematic representation of the sliding mode. The polarization and strain profiles are shifted by dx. (c),(d) Simulated strain profiles shown on a slice of the sample when the tip is near the DW (c) or further away (d). The dashed vertical line shows the initial position of the ferroelectric DW. The wall slides toward the tip in (c), as shown by the curved dashed line, whereas it does not move in (d).

studies of $BaTiO_3$ [51]. The contact of the CRFM tip with the surface is simulated by applying a bell-shaped force $\propto a\exp[-(x^2/d^2)]$, with $2d \sim 20$ nm representing the diameter of the contact area of the tip and $a = 10^{-7}$ J/m^3. The softening is estimated as the ratio of maximum deformation induced by the tip at the wall and in the domain. In order to stay within a linear regime and avoid polarization domain switching, the virtual force applied to the tip is kept very low, less than a femto-Newton.

These calculations predict that the elastic cost of deformation is smallest not at the domain wall itself, which is already spontaneously compressed and, thus, it is hard to compress further, but adjacent to it, where compression is achieved by the bending of the domain wall (and its accompanying depression) toward the tip [Fig. 4(a)]. As the tip moves further away, the distance becomes big enough that the stress field of the tip does not interact with the wall, and the material recovers its intrinsic stiffness.

In conclusion, the local stress induced by the tip can lead to a reversible (elasticlike) shift of domain walls. This sliding of the wall, with its associated "strain dip," contributes the local deformation (softening) of the material. Bassiri-Gharb *et al.* [24,25] show that the reversible motion of ferroelectric walls under applied electric fields has consequences for strain. Here, we observe a somewhat complementary effect: The domain walls are moved not by a homogeneous electric field, but by an inhomogeneous mechanical stress, resulting in a local change of strain.

Another contribution to mechanical contrast is depolarization. Applying tip pressure to the surface of a piezoelectric (all ferroelectrics are piezoelectric) by definition modifies its polarization and, thus, has an electrostatic energy cost. The AFM tip induces deformations ε_{ij} that are inhomogeneous (large near the tip, small far from the tip), so the polarization due to piezoelectricity, $P_i \sim e_{ijk}\varepsilon_{jk}$, is not homogeneous. Tip pressure, therefore, induces bound charges $\nabla \cdot P \neq 0$ in the inhomogeneously deformed region, and these create a depolarizing field. Higher depolarization implies bigger work and, thus, higher effective stiffness.

We identify two main mechanisms of formation of bound charges under the tip: (i) variation of in-plane polarization, $\nabla_1 P_1 \neq 0$, induced by shear piezoelectricity $P_1 \sim e_{15}\varepsilon_5$ [Fig. 5(a)], and (ii) generation of out-of-plane polarization due to longitudinal piezoelectricity, $\Delta P_3 \sim e_{11}\varepsilon_3$, which is unscreened in the case of open boundary conditions and screened at short-circuit conditions [Fig. 5(b)].

Because all the piezoelectric constants e_{jm} flip their signs across the domain wall, $e_{jm}(P_3\downarrow) = -e_{jm}(P_3\uparrow)$, the distribution of the tip-induced bound charges is qualitatively different when the tip is pressed at the domain and at the domain wall. For the charges induced by the "in-plane" mechanism [Fig. 5(a)], the in-plane polarization $P_1 \sim e_{15}\varepsilon_5$ forms a head-to-head or tail-to-tail pattern with

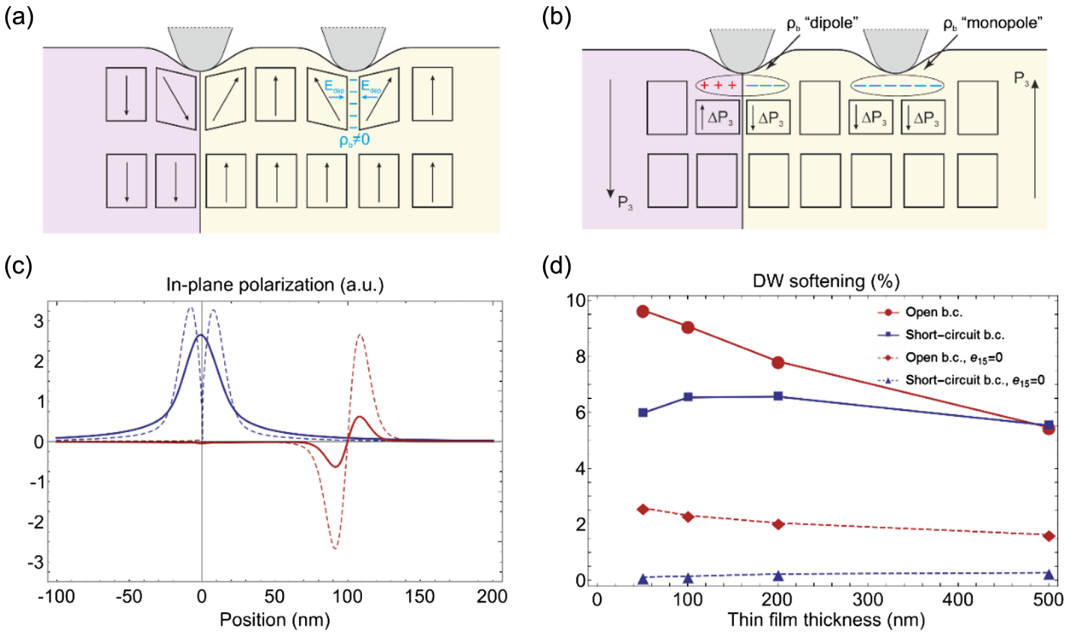

FIG. 5. (a) Schematic of the "in-plane" mechanism of the bound charge formation: Applying the tip to the surface induces in-plane polarization via the shear piezoelectricity: $P_1 \sim e_{15}\varepsilon_5$, with larger depolarizing electric fields E_{dep} when the tip is applied in the bulk domain. (b) Schematic of the "out-of-plane" mechanism of the domain wall softening: Applying the tip to the surface induces out-of-plane polarization $\Delta P_3 \sim e_{13}\varepsilon_1 + e_{33}\varepsilon_3$. (c) Manifestation of the depolarizing effect on the tip-induced in-plane polarization P_1. Solid lines: Polarization extracted from finite-element modeling at a distance 5 nm from the film surface, with the tip applied at the domain wall (blue) and in the bulk domain (red). Dashed lines: Polarization expected due to the shear piezoelectric effect $P_1 \approx e_{15}\varepsilon_5$, with shear strain ε_5 extracted at a distance 5 nm from the film surface. (d) Study of the domain wall softening at different electric boundary conditions, values of the shear piezoelectric coefficient e_{15}, and film thicknesses.

corresponding bound charges when the tip is pressed in the domain and a head-to-tail pattern when the tip is pressed at the domain wall, implying significantly reduced electrostatic energy costs and softer mechanical response in the latter case. Likewise, the surface charges generated by the "out-of-plane" mechanism [Fig. 5(b)] have monopolelike distribution when the tip is pressed in the domain and dipolelike distribution when the tip is pressed at the domain wall, again implying lower electrostatic energy costs and a softer mechanical response of the domain wall at open electric boundary conditions. Notice that this polarity-dependent orientation of the piezoelectric response is qualitatively different from flexoelectricity, which is polarity independent and, thus, less sensitive to the presence of a polar domain wall; for this reason, we discard flexoelectricity from the analysis.

We test the reasoning given above by modeling a simplified two-dimensional system, with the contact between the CRFM tip and the surface described by an out-of-plane force proportional to $e^{-(x^2/t^2)}$, where $2t \sim 20$ nm is the contact area. As in the experiment, we focus only on linear static elastic effects and apply a force small enough to avoid any polarization switching. All the simulations are done with two electric boundary conditions: open boundary conditions, with surface screening of the polarization by immobile surface charges (requiring the normal component of the electric displacement field at the surface $D_n = \epsilon_r E_n + P_n = P_S \tanh x/\xi$ at all times, where $\xi \sim 1$ nm), and short-circuit boundary conditions. We note that the experimentally investigated crystal is closer to the short-circuit case in the out-of-plane direction: Even though the film surface is not electroded, the AFM tip in contact with the surface is metallic.

In all studied cases, we obtain that, when the AFM tip is applied at the domain wall, the in-plane polarization P_1 generated under the tip [blue solid line in Fig. 5(c)] is described with good precision by the piezoelectric effect $P_1 \approx e_{15}\varepsilon_5$ [blue dashed line in Fig. 5(c)]. On the other hand, when the tip is applied in the bulk domain, the generated in-plane polarization is strikingly smaller to the one expected from piezoelectricity [Fig. 5(c), red lines]. This suppression of the in-plane polarization is due to the depolarizing cost of the head-to-head configuration and, as expected, is accompanied by a harder elastic response of the bulk domain compared to the domain wall. This difference translates into an apparent DW softening of 5%–10% [Fig. 5(d)] relative to the stiffness of the domain.

To confirm the link between the suppression of in-plane polarization and elastic hardening of the bulk, we also perform an additional simulation with the shear piezoelectric constant $e_{15} = 0$ [by setting the shear electrostriction coefficient $q_{44} = 0$ in Eq. (10)] at *short-circuit*

boundary conditions, thus removing both the bound charges appearing in plane and out of plane. As a result, the DW softening almost vanishes, down to <0.3% [Fig. 5(d)] (here, in-plane refers to the plane of the film, not the wall). Then, reactivating the in-plane mechanism of charge formation by returning e_{15} to the $BaTiO_3$ value leads to an averaged 6% increase of the DW softening, and applying open boundary conditions increases the DW softening by another 2% [Fig. 5(d)]. The somewhat surprising conclusion, therefore, is that the main contributor to the electrostatic softening at the wall is *not* the out-of-plane piezoelectricity but the in-plane (shear) piezoelectricity. This result is important because, while the former can be partially screened by the use of metallic tips or in the presence of electrodes or adsorbates, the latter cannot. The in-plane piezoelectric contribution to domain wall softening is therefore unavoidable, despite the polar axis being out of plane.

The aforementioned mechanisms (inhomogeneous piezoelectricity and sliding of the domain wall's strain dip) have a strong effect on only the effective vertical elastic compliance (S_{33}), but not on S_{11} and S_{22}. The domain wall softening is thus anisotropic, a result supported by the experimental observation [Fig. 3(c)] that the mechanical resonance frequency is slower at the 180° DW in *c* domains but unaffected when the same 180° domain walls are measured in plane across *a* domains.

It is also important to emphasize that the effective elastic properties measured under inhomogeneous strain do not directly equate to the components of the linear elastic tensor measured under homogeneous stress. The total elastic energy incorporating both the standard Hooke's law component plus gradient elasticity is $U = 1/2E\varepsilon^2 + 1/2K(\nabla\varepsilon)^2$ [56–58], where K is the gradient coefficient that relates the mechanical energy to the strain gradient. In our model, we have subsumed both K and E (the Young's modulus) within an effective elastic constant E^*, but this constant should not be confused with the real Young's modulus. The gradient elasticity is as much a mechanical property of the material as the linear elasticity described by E, but it is apparent only under strongly inhomogeneous deformations.

V. CONCLUSIONS

Although ferroelectric 180° domains are mechanically identical, the domain walls that separate them display mechanical contrast: The walls are softer than the domains. This softening is detected as a lowering of the mechanical resonance frequency of the AFM cantilever in contact with the domain wall. This result has been reiterated here on single crystals of uniaxial lithium niobate and perovskite $BaTiO_3$ and epitaxial thin films of $PbTiO_3$, in addition to ceramics of lead zirconate-titanate [30,31]. The effect, therefore, appears to be general and not dependent on material composition or sample morphology. Theoretical modeling shows that there can be at least two contributing factors: domain wall sliding and depolarization-activated electromechanical coupling. For $BaTiO_3$, these two contributions have a quantitatively comparable impact on the total softening. Ferroelectric 180° domain walls have, by definition, $P = 0$ in the vertical direction, so the spontaneous strain associated with P is suppressed at the wall, resulting in a "strain dip" near the surface. When an inhomogeneous vertical compression is delivered by the AFM tip near the wall, therefore, the material can respond by sliding (or broadening) the wall so that this region of inherently reduced vertical strain (also known as strain dip) moves under the tip. This dynamic response requires the strain field from the tip to be inhomogeneous and asymmetrically located with respect to the wall; if there is the same amount of compression on either side of the wall, it does not move. However, it is important to emphasize that this effect is not flexoelectric.

It is also worth noticing that the strain dip is not topographically observable. The pseudocubic relaxation affects only the near-surface unit cells; deeper into the film, the domain wall unit cells are fully clamped to those of the adjacent domains and, thus, cannot relax. The calculated depth of the dip is <1 Å, and the width is approximately 1 nm (standard width of a 180° wall), well below the topographical detection limit of the AFM. Though this deformation is itself not observable, however, its mechanical consequences are. On the other hand, this elastic response is effective only in the surface, so it cannot be considered a bulk elastic property. The only softening mechanism that is effective along the entire domain wall is the one due to inhomogeneous piezoelectricity.

The depolarization field generated upon inhomogeneously straining a piezoelectric material contributes to its gradient elasticity—making the material stiffer. Tip-induced inhomogeneous deformation generates in-plane piezoelectric polarization via a shear piezoelectric effect. In a tetragonal ferroelectric, this in-plane component must be head to head or tail to tail in the domains, whereas it is head to tail in the domain walls—hence, the electrostatic costs are smaller at the domain walls, which facilitates their deformation. However, this type of polarization discontinuity accompanies any inhomogeneous deformation in a piezoelectric material, so its mechanical effect is not limited to tip-induced indentations. Such electrostatic effects accompany any modulation of the lattice, such as phonons.

The fact that purely ferroelectric (i.e., nonferroelastic) domain walls display mechanical contrast with respect to their surroundings has obvious consequences for the mechanical properties of the material. It also has functional consequences. Mechanical reading of ferroelectric polarity is possible, but the mechanical contrast between domains is weak [23], whereas the mechanical contrast of the domain walls is much clearer and offers an easier way to "read" ferroelectric bits, being a potential basis for phononic switches [21,22]. In this respect, the mechanical contrast

at the wall means that periodically poled ferroelectric crystals can also be regarded as phononic crystals. The more general lesson is that domain walls are distinct not only functionally, but also mechanically, and the complete picture of domain wall physics must incorporate this mechanical singularity.

ACKNOWLEDGMENTS

C. S. thanks BIST for the PREBIST Grant. This project has received funding from the European Union's Horizon 2020 research and innovation program under the Marie Skłodowska-Curie Grant Agreement No. 754558. E. L. acknowledges the funding received from the European Union's Horizon 2020 research and innovation program through the Marie Skłodowska-Curie Actions: Individual Fellowship-Global Fellowship (Ref. No. MSCA-IF-GF-708129). M. S. and K. S. acknowledge the support of the European Research Council under the European Union's Horizon 2020 research and innovation program (Grant Agreement No. 724529), Ministerio de Economia, Industria y Competitividad through Grants No. MAT2016-77100-C2-2-P and No. SEV-2015-0496, and the Generalitat de Catalunya (Grant No. 2017SGR 1506). G. C. acknowledge the support of the Ministerio de Economía, Industria y Competitividad, Agencia Estatal de Investigación/Fondo Europeo de Desarrollo Regional and European Union through Grant No. MAT2016-77100-C2-1-P (MINECO/AEI/FEDER, UE).

[1] J. Seidel, L. W. Martin, Q. He, Q. Zhan, Y. H. Chu, A. Rother, M. E. Hawkridge, P. Maksymovych, P. Yu, M. Gajek, N. Balke, S. V Kalinin, S. Gemming, F. Wang, G. Catalan, J. F. Scott, N. A. Spaldin, J. Orenstein, and R. Ramesh, *Conduction at Domain Walls in Oxide Multiferroics*, Nat. Mater. **8**, 229 (2009).

[2] S. Farokhipoor and B. Noheda, *Conduction through 71° Domain Walls in* $BiFeO_3$ *Thin Films*, Phys. Rev. Lett. **107**, 127601 (2011).

[3] Q. He, C. H. Yeh, J. C. Yang, G. Singh-Bhalla, C. W. Liang, P. W. Chiu, G. Catalan, L. W. Martin, Y. H. Chu, J. F. Scott, and R. Ramesh, *Magnetotransport at Domain Walls in* $BiFeO_3$, Phys. Rev. Lett. **108**, 067203 (2012).

[4] J. H. Lee, I. Fina, X. Marti, Y. H. Kim, D. Hesse, and M. Alexe, *Spintronic Functionality of* $BiFeO_3$ *Domain Walls*, Adv. Mater. **26**, 7078 (2014).

[5] N. M. Murari, S. Hong, H. N. Lee, and R. S. Katiyar, *Direct Observation of Fatigue in Epitaxially Grown* $Pb(Zr, Ti)O_3$ *Thin Films Using Second Harmonic Piezoresponse Force Microscopy*, Appl. Phys. Lett. **99**, 052904 (2011).

[6] A. Aird and E. K. H. Salje, *Sheet Superconductivity in Twin Walls: Experimental Evidence of* WO_{3-x}, J. Phys. Condens. Matter **10**, L377 (1998).

[7] J. Guyonnet, I. Gaponenko, S. Gariglio, and P. Paruch, *Conduction at Domain Walls in Insulating* $Pb(Zr_{0.2}Ti_{0.8})O_3$ *Thin Films*, Adv. Mater. **23**, 5377 (2011).

[8] M. Schröder, A. Haußmann, A. Thiessen, E. Soergel, T. Woike, and L. M. Eng, *Conducting Domain Walls in Lithium Niobate Single Crystals*, Adv. Funct. Mater. **22**, 3936 (2012).

[9] T. Choi, Y. Horibe, H. T. Yi, Y. J. Choi, W. Wu, and S. W. Cheong, *Insulating Interlocked Ferroelectric and Structural Antiphase Domain Walls in Multiferroic* $YMnO_3$, Nat. Mater. **9**, 253 (2010).

[10] R. G. P. McQuaid, M. P. Campbell, R. W. Whatmore, A. Kumar, and J. Marty, *Gregg Injection and Controlled Motion of Conducting Domain Walls in Improper Ferroelectric Cu-Cl Boracite*, Nat. Commun. **8**, 15105 (2017).

[11] D. Meier, *Functional Domain Walls in Multiferroics*, J. Phys. Condens. Matter **27**, 463003 (2015).

[12] G. Catalan, J. Seidel, R. Ramesh, and J. F. Scott, *Domain Wall Nanoelectronics*, Rev. Mod. Phys. **84**, 119 (2012).

[13] E. K. H. Salje, *Multiferroic Domain Boundaries as Active Memory Devices: Trajectories towards Domain Boundary Engineering*, ChemPhysChem **11**, 940 (2010).

[14] J. Muñoz-Saldaña, G. A. Schneider, and L. M. Eng, *Stress Induced Movement of Ferroelastic Domain Walls in* $BaTiO_3$ *Single Crystals Evaluated by Scanning Force Microscopy*, Surf. Sci. **480**, L402 (2001).

[15] V. Anbusathaiah, D. Kan, F. C. Kartawidjaja, R. Mahjoub, M. A. Arredondo, S. Wicks, I. Takeuchi, J. Wang, and V. Nagarajan, *Labile Ferroelastic Nanodomains in Bilayered Ferroelectric Thin Films*, Adv. Mater. **21**, 3497 (2009).

[16] T. Y. Zhang and C. F. Gao, *Fracture Behaviors of Piezoelectric Materials*, Theor. Appl. Fract. Mech. **41**, 339 (2004).

[17] A. Abdollahi and I. Arias, *Phase-Field Modeling of Crack Propagation in Piezoelectric and Ferroelectric Materials with Different Electromechanical Crack Conditions*, J. Mech. Phys. Solids **60**, 2100 (2012).

[18] S. M. Park, B. Wang, S. Das, S. C. Chae, J. S. Chung, J. G. Yoon, L. Q. Chen, S. M. Yang, and T. W. Noh, *Selective Control of Multiple Ferroelectric Switching Pathways Using a Trailing Flexoelectric Field*, Nat. Nanotechnol. **13**, 366 (2018).

[19] K. Shapovalov, P. V. Yudin, A. K. Tagantsev, E. A. Eliseev, A. N. Morozovska, and N. Setter, *Elastic Coupling between Nonferroelastic Domain Walls*, Phys. Rev. Lett. **113**, 207601 (2014).

[20] E. Langenberg, D. Saha, M. E. Holtz, J. J. Wang, D. Bugallo, E. Ferreiro-Vila, H. Paik, I. Hanke, S. Ganschow, D. A. Muller, L. Q. Chen, G. Catalan, N. Domingo, J. Malen, D. G. Schlom, and F. Rivadulla, *Ferroelectric Domain Walls in* $PbTiO_3$ *are Effective Regulators of Heat Flow at Room Temperature*, Nano Lett. **19**, 7901 (2019).

[21] J. A. Seijas-Bellido, C. Escorihuela-Sayalero, M. Royo, M. P. Ljungberg, J. C. Wojdeł, J. Íñiguez, and R. Rurali, *A Phononic Switch Based on Ferroelectric Domain Walls*, Phys. Rev. B **96**, 140101 (2017).

[22] J. F. Ihlefeld, B. M. Foley, D. A. Scrymgeour, J. R. Michael, B. B. McKenzie, D. L. Medlin, M. Wallace,

S. Trolier-Mckinstry, and P. E. Hopkins, *Room-Temperature Voltage Tunable Phonon Thermal Conductivity via Reconfigurable Interfaces in Ferroelectric Thin Films*, Nano Lett. **15**, 1791 (2015).

[23] K. Cordero-Edwards, N. Domingo, A. Abdollahi, J. Sort, and G. Catalan, *Ferroelectrics as Smart Mechanical Materials*, Adv. Mater. **29**, 1702210 (2017).

[24] N. Bassiri-Gharb, S. Trolier-Mckinstry, and D. Damjanovic, *Strain-Modulated Piezoelectric and Electrostrictive Nonlinearity in Ferroelectric Thin Films without Active Ferroelastic Domain Walls*, J. Appl. Phys. **110**, 124104 (2011).

[25] S. Trolier-McKinstry, N. B. Gharb, and D. Damjanovic, *Piezoelectric Nonlinearity due to Motion of 180° Domain Walls in Ferroelectric Materials at Subcoercive Fields: A Dynamic Poling Model*, Appl. Phys. Lett. **88**, 202901 (2006).

[26] R. L. Johnson-Wilke, R. H. T. Wilke, M. Wallace, A. Rajashekhar, G. Esteves, Z. Merritt, J. L. Jones, and S. Trolier-Mckinstry, *Ferroelectric/Ferroelastic Domain Wall Motion in Dense and Porous Tetragonal Lead Zirconate Titanate Films*, IEEE Trans. Ultrason. Ferroelectr. Freq. Control **62**, 46 (2015).

[27] V. Anbusathaiah, S. Jesse, M. A. Arredondo, F. C. Kartawidjaja, O. S. Ovchinnikov, J. Wang, S. V. Kalinin, and V. Nagarajan, *Ferroelastic Domain Wall Dynamics in Ferroelectric Bilayers*, Acta Mater. **58**, 5316 (2010).

[28] F. Xu, S. Trolier-McKinstry, W. Ren, B. Xu, Z. L. Xie, and K. J. Hemker, *Domain Wall Motion and Its Contribution to the Dielectric and Piezoelectric Properties of Lead Zirconate Titanate Films*, J. Appl. Phys. **89**, 1336 (2001).

[29] D. Damjanovic and M. Demartin, *Contribution of the Irreversible Displacement of Domain Walls to the Piezoelectric Effect in Barium Titanate and Lead Zirconate Titanate Ceramics*, J. Phys. Condens. Matter **9**, 4943 (1997).

[30] T. Tsuji, S. Saito, K. Fukuda, K. Yamanaka, H. Ogiso, J. Akedo, and Y. Kawakami, *Significant Stiffness Reduction at Ferroelectric Domain Boundary Evaluated by Ultrasonic Atomic Force Microscopy*, Appl. Phys. Lett. **87**, 071909 (2005).

[31] T. Tsuji, H. Ogiso, J. Akedo, S. Saito, K. Fukuda, and K. Yamanaka, *Evaluation of Domain Boundary of Piezo/Ferroelectric Material by Ultrasonic Atomic Force Microscopy*, Jpn. J. Appl. Phys. **43**, 2907 (2004).

[32] P. Ferraro, S. Grilli, and P. De Natale, *Ferroelectric Crystals for Photonic Applications: Including Nanoscale Fabrication and Characterization Techniques*, second ed., Springer Series in Materials Science (Springer, New York, 2014).

[33] U. Rabe, S. Amelio, E. Kester, V. V. Scherer, S. Hirsekorn, and W. Arnold, *Quantitative Determination of Contact Stiffness Using Atomic Force Acoustic Microscopy*, Ultrasonics **38**, 430 (2000).

[34] See Supplemental Material at http://link.aps.org/supplemental/10.1103/PhysRevX.10.041001 for experimental details and clarifications.

[35] C. Harnagea, A. Pignolet, M. Alexe, and D. Hesse, *Piezoresponse Scanning Force Microscopy: What Quantitative Information Can We Really Get Out of Piezoresponse Measurements on Ferroelectric Thin Films*, Integr. Ferroelectr. **44**, 113 (2002).

[36] E. Soergel, *Piezoresponse Force Microscopy (PFM)*, J. Phys. D **44**, 464003 (2011).

[37] X. K. Wei, C. L. Jia, T. Sluka, B. X. Wang, Z. G. Ye, and N. Setter, *Néel-like Domain Walls in Ferroelectric* $Pb(Zr, Ti)O_3$ *Single Crystals*, Nat. Commun. **7**, 12385 (2016).

[38] G. De Luca, M. D. Rossell, J. Schaab, N. Viart, M. Fiebig, and M. Trassin, *Domain Wall Architecture in Tetragonal Ferroelectric Thin Films*, Adv. Mater. **29**, 1605145 (2017).

[39] J. C. Wojdeł and J. Íñiguez, *Ferroelectric Transitions at Ferroelectric Domain Walls Found from First Principles*, Phys. Rev. Lett. **112**, 247603 (2014).

[40] S. Cherifi-Hertel, H. Bulou, R. Hertel, G. Taupier, K. D. H. Dorkenoo, C. Andreas, J. Guyonnet, I. Gaponenko, K. Gallo, and P. Paruch, *Non-Ising and Chiral Ferroelectric Domain Walls Revealed by Nonlinear Optical Microscopy*, Nat. Commun. **8**, 15768 (2017).

[41] S. Kim, V. Gopalan, and A. Gruverman, *Coercive Fields in Ferroelectrics: A Case Study in Lithium Niobate and Lithium Tantalate*, Appl. Phys. Lett. **80**, 2740 (2002).

[42] K. Cordero-Edwards, H. Kianirad, C. Canalias, J. Sort, and G. Catalan, *Flexoelectric Fracture-Ratchet Effect in Ferroelectrics*, Phys. Rev. Lett. **122**, 135502 (2019).

[43] A. Abdollahi, C. Peco, D. Millán, M. Arroyo, G. Catalan, and I. Arias, *Fracture Toughening and Toughness Asymmetry Induced by Flexoelectricity*, Phys. Rev. B **92**, 094101 (2015).

[44] U. Rabe, S. Amelio, M. Kopycinska, S. Hirsekorn, M. Kempf, M. Göken, and W. Arnold, *Imaging and Measurement of Local Mechanical Material Properties by Atomic Force Acoustic Microscopy*, Surf. Interface Anal. **33**, 65 (2002).

[45] W. C. Oliver and F. R. Brotzen, *On the Generality of the Relationship among Contact Stiffness, Contact Area, and Elastic Modulus during Indentation*, J. Mater. Res. **7**, 1564 (1992).

[46] U. Rabe and W. Arnold, *Atomic Force Microscopy at MHz Frequencies*, Ann. Phys. (N.Y.) **506**, 589 (1994).

[47] D. C. Hurley, *Contact Resonance Force Microscopy Techniques for Nanomechanical Measurements, Applied Scanning Probe Methods XI: Scanning Probe Microscopy Techniques*, (Springer, Berlin, 2009).

[48] U. Rabe, M. Kopycinska-Müller, and S. Hirsekorn, *Atomic Force Acoustic Microscopy*, in Acoustic Scanning Probe Microscopy, edited by F. Marinello, D. Passeri, and E. Savio (Springer, Berlin, 2013).

[49] J. A. Turner, S. Hirsekorn, U. Rabe, and W. Arnold, *High-Frequency Response of Atomic-Force Microscope Cantilevers*, J. Appl. Phys. **82**, 966 (1997).

[50] D. Berlincourt and H. Jaffe, *Elastic and Piezoelectric Coefficients of Single-Crystal Barium Titanate*, Phys. Rev. **111**, 143 (1958).

[51] P. Marton, I. Rychetsky, and J. Hlinka, *Domain Walls of Ferroelectric* $BaTiO_3$ *within the Ginzburg-Landau-Devonshire Phenomenological Model*, Phys. Rev. B **81**, 144125 (2010).

[52] J. Hlinka and P. Márton, *Phenomenological Model of a 90° Domain Wall in* $BaTiO_3$*-Type Ferroelectrics*, Phys. Rev. B **74**, 104104 (2006).

[53] L. Zheng, K. Lai, R. Hu, Y. Ren, U. Petralanda, X. Wu, S.-W. Cheong, and S. Artyukhin, *Low-Energy Structural*

Dynamics of Ferroelectric Domain Walls in Hexagonal Rare-Earth Manganites, Sci. Adv. **3**, e1603229 (2017).

[54] J. Hlinka, M. Paściak, S. Körbel, and P. Marton, *Terahertz-Range Polar Modes in Domain-Engineered* $BiFeO_3$, Phys. Rev. Lett. **119**, 057604 (2017).

[55] S. Prosandeev, Y. Yang, C. Paillard, and L. Bellaiche, *Displacement Current in Domain Walls of Bismuth Ferrite*, npj Comput. Mater. **4**, 8 (2018).

[56] R. Maranganti and P. Sharma, *A Novel Atomistic Approach to Determine Strain-Gradient Elasticity Constants: Tabulation and Comparison for Various Metals, Semiconductors, Silica, Polymers and the (Ir) Relevance for Nanotechnologies*, J. Mech. Phys. Solids **55**, 1823 (2007).

[57] D. C. C. Lam, F. Yang, A. C. M. Chong, J. Wang, and P. Tong, *Experiments and Theory in Strain Gradient Elasticity*, J. Mech. Phys. Solids **51**, 1477 (2003).

[58] M. Stengel, *Unified Ab Initio Formulation of Flexoelectricity and Strain-Gradient Elasticity*, Phys. Rev. B **93**, 245107 (2016).

Supplementary Information

MECHANICAL SOFTNESS OF FERROELECTRIC 180 DEGREE DOMAIN WALLS

Christina Stefani[1], Louis Ponet[2, 3], Konstantin Shapovalov[4], Peng Chen[2], Eric Langenberg[5], Darrell G. Schlom[5, 6] Sergey Artyukhin [2], Massimiliano Stengel[4, 7], Neus Domingo[1], Gustau Catalan[1, 7]

[1] *ICN2-Institut Català de Nanociència I Nanotecnologia (CERCA-BIST-CSIC), Campus Universitat Autònoma de Barcelona, Bellaterra, Catalonia*
[2] *Italian Institute of Technology, 16163 Genoa GE, Italy*
[3] *Scuola Normale Superiore di Pisa, 56126 Pisa PI Italy*
[4] *ICMAB-Institut de Ciència de Materials de Barcelona, Bellaterra, Catalonia*
[5] *Department of Materials Science and Engineering, Cornell University, Ithaca, New York 14853, USA*
[6] *Kavli Institute at Cornell for Nanoscale Science, Ithaca, New York 14853, USA*
[7] *ICREA-Catalan Institution for Research and Advanced Studies, Passeig Lluïs Companys, Barcelona, Catalonia*

1. Experimental Methods.

DART PFM: PFM measures the mechanical response when an AC voltage is applied to the sample, through an electrically conductive tip in contact. In response to the voltage, the sample locally expands or contracts and the local piezoelectric response is detected through the deflection of the cantilever, and the phase φ yields information about the direction of the sample's polarization. In dual AC resonance tracking mode (DART)[1,2] the resonance frequency tracking is based on the use of two closely spaced excitation frequencies, one below (f_1) and one above (f_2) the resonance frequency (f_r). The motion of the cantilever is measured and sent to two separate lock-in amplifiers, each referenced to one of the drive signals, measuring the resulting amplitudes and frequencies (f_1, A_1, f_2, A_2). When there is a shift in resonance frequency, the amplitude signals become different (A_2-$A_1 \neq 0$, as shown in Fig. 1b). A feedback loop is used to maintain A_2-A_1=0, and thus track the resonance frequency.

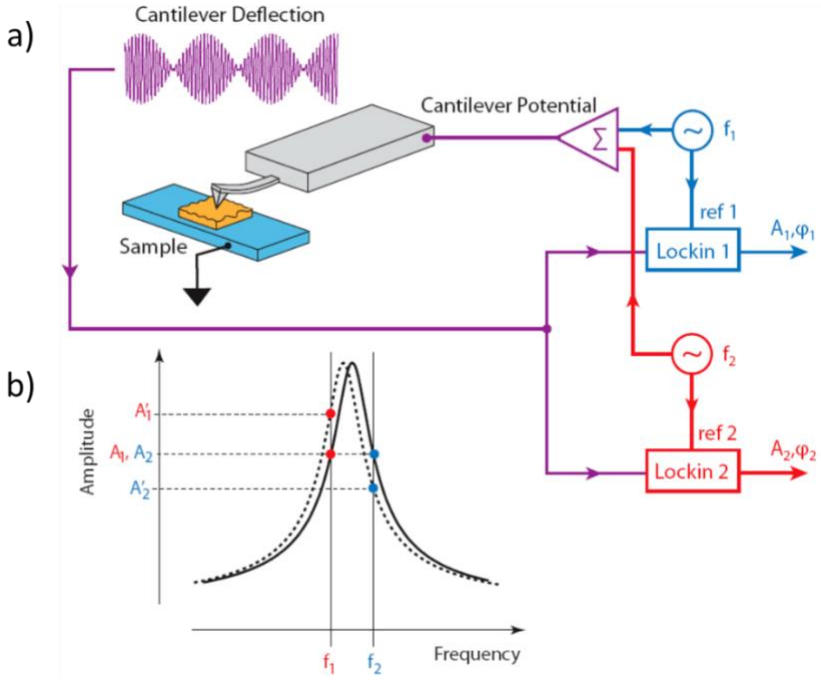

Figure 1. (a) Schematic diagram of the experimental setup[2], *(b) Solid and dash lines represent the amplitudes and frequencies measures before and after a shift in resonance frequency*

CR-FM: Contact Resonance Force Microscopy directly measures the tip-sample mechanical coupling by tracking the mechanical contact resonance. The tip is in contact with the sample, but it does not excite the sample electrically, as in PFM. Instead, the system is mechanically excited from the top, through a piezo element placed at the base of the cantilever or from the bottom, using an acoustic stage under the sample[3]. The frequency of the oscillation is modulated until mechanical resonance is reached, and it is tracked using the same DART approach as for PFM. The resonant frequency of the system depends both on the geometrical characteristics of the tip and the tip-sample mechanical contact characteristics. We assume that the characteristics of the tip remain the same through the whole measurement. During the scanning process, the force between the tip and the sample is being kept constant, and the frequency response of the tip-sample coupled system is measured. Due to the fact that changes of resonant frequency are caused because of changes in tip-sample mechanical contact, shifts in the measured frequency are proportional with the stiffness of the sample.

Most of the measurements presented in this paper are done using cantilever excitation, but we have compared both technical approaches. In order to ensure that the results are valid, we performed the same CR-FM experiments by mechanically exciting the cantilever and compared the results with those obtained using an acoustic stage: while there is a significant difference in the signal of noise ratio as expected, being the results obtained using an acoustic stage quantitatively better, both show the same qualitative behavior, as shown in Fig. 2.

Supplementary Information

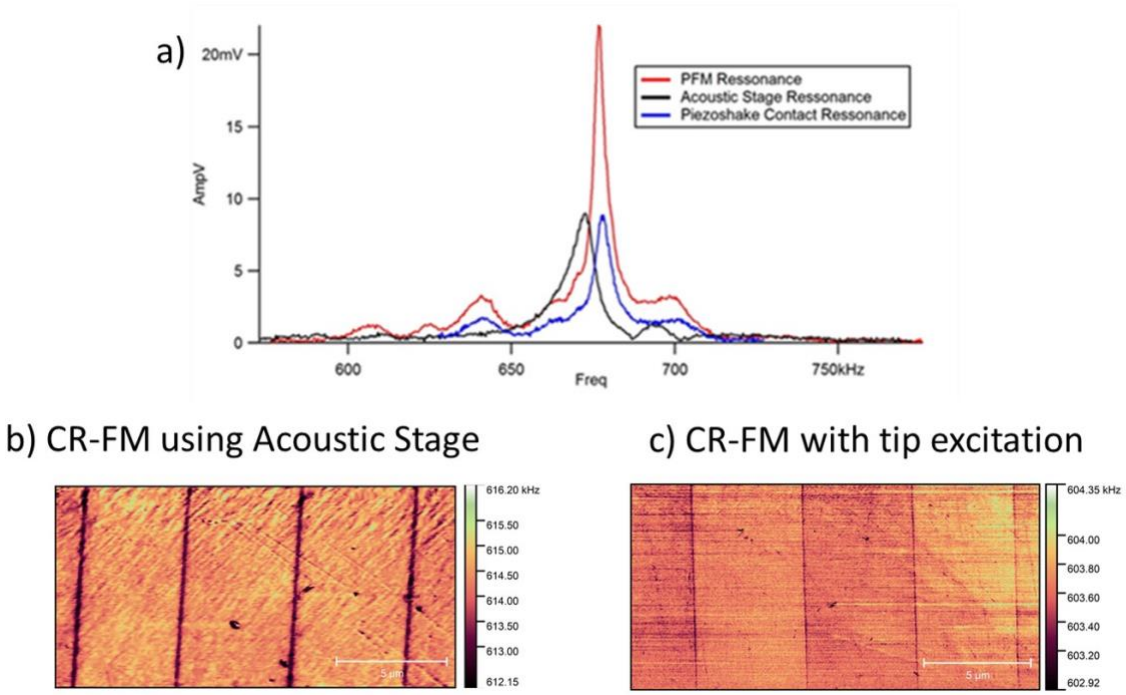

Figure 2: (a) Comparison of the contact resonance using three different modes: piezoelectric excitation, mechanical excitation using an acoustic stage and mechanical excitation vibrating the tip. The cantilever used here was an OMCL-AC240TM, from Olympus, and the sample corresponds to PPLN. (b), (c)While the images for the Acoustic stage show a higher quality with lower signal to noise ratio, both type of excitations lead to qualitatively and quantitatively the same results

2. CR-FM as a function of cantilever stiffness.

The system of the cantilever in contact with the sample, in the case of CR-FM experiments, can be described as a system of two springs in series. The first spring represents the cantilever and the second one the mechanical contact of the tip and the sample (Fig.2 of the manuscript). In order to be able to measure changes in the mechanical properties of the sample, both springs must have similar stiffness. If the cantilever's spring constant is much smaller than the sample's, then most of the mechanical energy of the vibration corresponds to the cantilever and the resonant frequency becomes almost insensitive to the mechanical properties of the sample. Figure 3 demonstrates CR-FM experiments made on $LiNbO_3$ sample with cantilevers of different stiffness. It is clear that in the case of the soft cantilever (k~3 N/m), the contrast in frequency is in the limit of detectable differences.

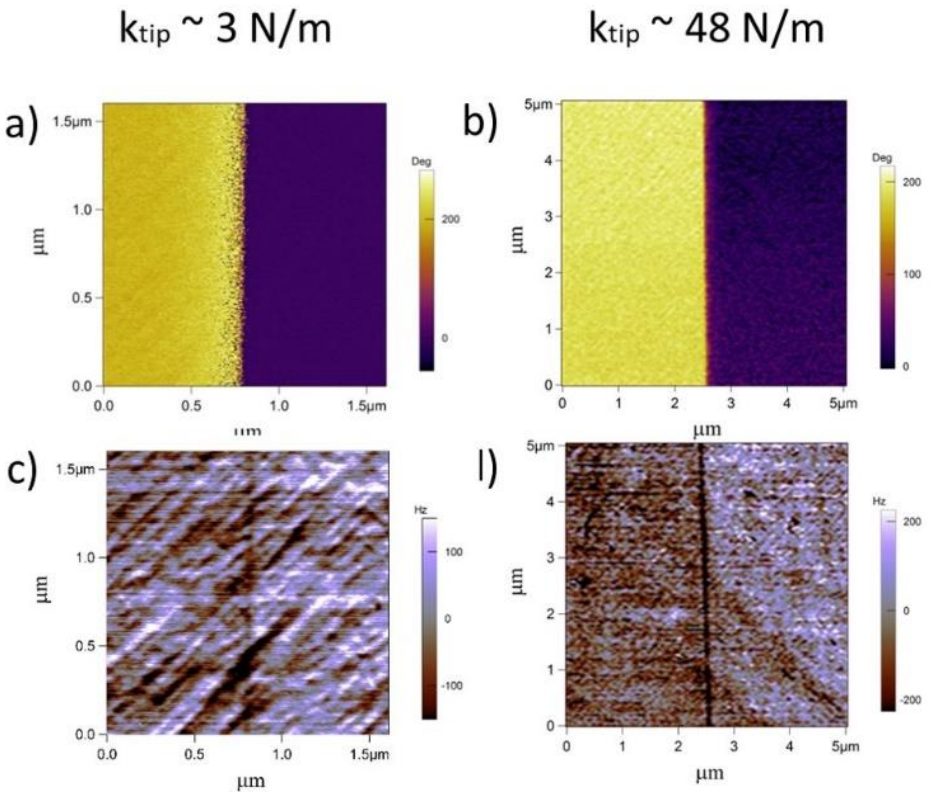

Figure 3. $LiNbO_3$ measured by cantilevers with different stiffness. (a) and (b) demonstrate the corresponding DART PFM image showing areas with opposite out of plane polarization and (c),(d) are the corresponding CR-FM images. In the case of the soft cantilever (left side) the contrast in frequency shift is much smaller.

3. Stability of ferroelectric domains with scanning

The ferroelectric domains observed in the different materials showed high stability after several scans under different applied forces. Systematically we checked the ferroelectric domain shapes with PFM before and after every CR-FM measurement to probe that the domain wall position was stable over the mechanical imaging, probing the absence of mechanically induced switching.

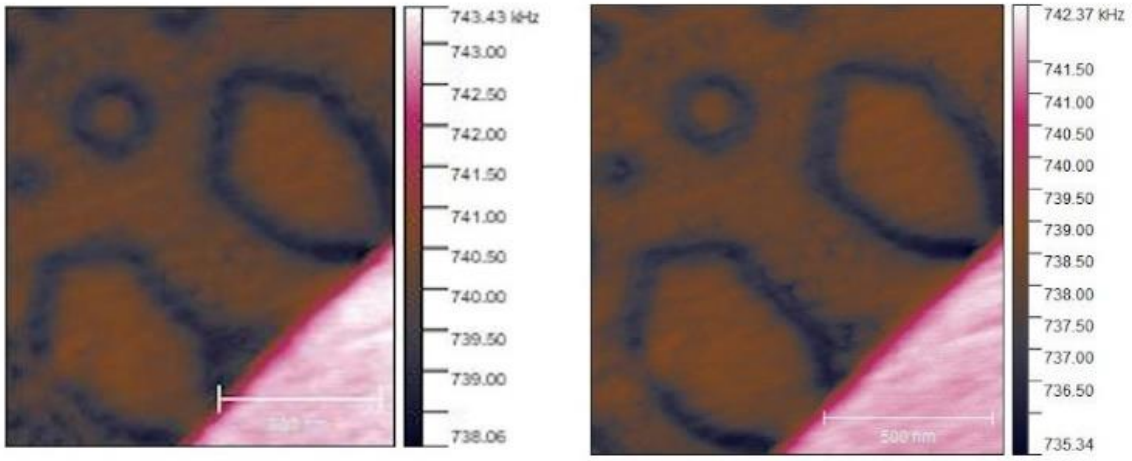

Figure 4: comparison between the domain configuration of the BTO crystal during the first slow scan (left) and the 10th (right), showing no evidence of mechanically-induced switching.

4. In-plane ferroelectric domains configuration.

The presence of in-plane ferroelectric domains in BaTiO3 single crystals was studied using Lateral-PFM measurements. Its presence was clearly observed as a high amplitude in the signal of LPFM images.

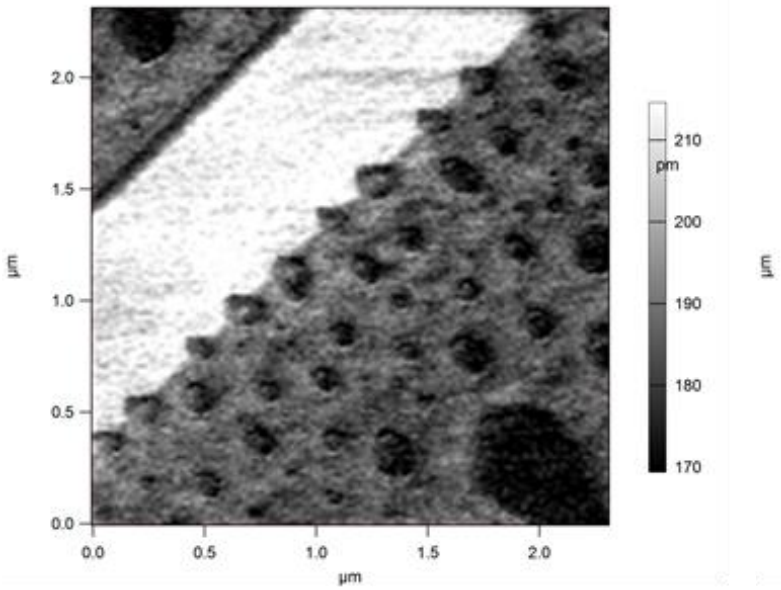

Figure 5. Amplitude of lateral PFM signal for $BaTiO_3$ single crystal. The lateral PFM shows maximum amplitude in the a-domain (as expected), which shows as a diagonal white stripe. The out-of-plane c-domain is darker (lower amplitude), also as expected. The contrast is reversed in vertical PFM. The domain walls of the 180 degree bubble domains appear, if anything, even darker. There is therefore no evidence of an in-plane component of the piezoelectric tensor at the walls (i.e., no evidence of in-plane polarization at the walls).

Supplementary Information

5. On the origin of the contrast in mechanical response.

The measurements of elastic contrast (resonance frequency difference) yield a smaller value for the $BaTiO_3$ single crystal compared to the $PbTiO_3$ films despite the fact that $BaTiO_3$ actually has a higher shear piezoelectric coefficient than $PbTiO_3$, and hence one might expect a bigger softening of the wall for BTO than for PTO –if shear piezoelectricity is the main contributor.

As discussed in the paper, there are at least two factors contributing to the softer mechanical response of 180-degree domain walls: the electrostatic cost of the shear-induced head-to-head polarization and the spontaneous compression of the wall due to the absence of polarization. This compression is directly proportional to the tetragonality of the lattice and is therefore bigger for $PbTiO_3$. So, it is possible that the sum of shear piezoelectricity and compression is bigger for $PbTiO_3$ than for $BaTiO_3$.

A second explanation though plays an important role. What we measure experimentally is the resonance frequency of the cantilever, which results from the convolution between the flexural elastic constant of the cantilever and the Young's modulus of the sample. The system behaves as two springs in series, where the softer spring (which is the one that dominates the effective spring constant and hence the resonance frequency) is in fact the cantilever's. The relative impact of the sample on the total resonance frequency is inversely proportional to the stiffness of the sample: for an infinitely stiff sample, all we would measure is the mechanical response of the cantilever, while, conversely, for an infinitely stiff cantilever, only the sample would deform. Therefore, if one of the materials is softer than the other to start with, any change in its mechanical response will have proportionally a bigger impact on the measured resonance frequency. That is the case with $PbTiO_3$, which has an out-of-plane elastic constant of 30GPa[4], compared with 63,4 GPa for $BaTiO_3$ [5].

Concluding, only resonance differences within the same scan –on the same material- are meaningful, and even those need to be calibrated and processed to extract quantitative values.

References.

[1] A. Kalinin, S. V. Gruverman "Scanning Probe Microscopy for Functional Materials: Nanoscale Imaging and Spectroscopy", (2011).
[2] B.J. Rodriguez, C. Callahan, S. V. Kalinin, R. Proksch "Dual-frequency resonance-tracking atomic force microscopy", Nanotechnology 18(47) (2007).
[3] U. Rabe, M. Kopycinska-Müller, S. Hirsekorn "Atomic Force Acoustic Microscopy", in: F. Marinello, D. Passeri, E. Savio (Eds.), "Acoustic Scanning Probe Microscopy", Springer Berlin Heidelberg, Berlin, Heidelberg, (2013).
[4] A.G. Kalinichev, J.D. Bass, B.N. Sun, D.A. Payne "Elastic properties of tetragonal PbTiO3 single crystals by Brillouin scattering", J. Mater. Res. 12(10) (1997).
[5] D. Berlincourt, H. Jaffe "Elastic and Piezoelectric Coefficients of Single-Crystal Barium Titanate", Phys. Rev. 111(1) (1958).